

## Computational Study of New Isatin Molecules as Potential Thymidine Phosphorylase (TP) Inhibitors Against Cancer Activity. 3D-QSAR, Molecular Docking, ADME-Tox, And Molecular Dynamics Simulation Analysis

Reda EL-Mernissi<sup>1</sup>, Marwa Alaqarbeh<sup>2\*</sup>, Ayoub Khaldan<sup>1</sup>, Abdelouahid Sbai<sup>1</sup>, Mohammed Aziz Ajana<sup>1</sup>, Tahar Lakhlifi<sup>1</sup>, Mohammed Bouachrine<sup>1</sup>

<sup>1</sup>Molecular Chemistry and Natural Substances Laboratory, Faculty of Science, University of Moulay Ismail. Meknes. Morocco.

<sup>2</sup>Applied Science Research Center, Applied Science Private University, Jordan.

**\*Corresponding author:** Marwa Alaqarbeh, email: [marwaqarbh@hotmail.com](mailto:marwaqarbh@hotmail.com); [m\\_alaqarbeh@asu.edu.jo](mailto:m_alaqarbeh@asu.edu.jo)

Received December 5<sup>th</sup>, 2024; Accepted January 29<sup>th</sup>, 2025.

DOI: <http://dx.doi.org/10.29356/jmcs.v69i4.2150>

**Abstract.** The quenching of TP enzyme activity helps treat and control diseases. In this research, computational methods investigated a series of thirty isatin-based oxadiazoles as potential TP inhibitors. 3D-QSAR was used to design four isatins (A, B, C, and D) derivatives with high anticancer activity. Molecular Docking was used to investigate interaction types between designed isatin derivatives (A, B, C, and D) and the TP enzyme (PDB: 4EAD); the results show that all compounds have several types of exciting interactions with no unfavorable interactions, but only compounds A and B have conventional hydrogen bond interactions as promising inhibition activity. The Binding Energy between (A, B, C, and D) compounds with TP enzyme were obtained by molecular dynamic simulation at 100 ns. A and B compounds had a more substantial binding free energy than C and D compounds, with binding energies of -20.1374 +/- 0.1189 kJ/mol, -20.1897 +/- 0.1333 kJ/mol, -18.1344 +/- 0.1604 kJ/mol, and 19.077 +/- 0.1549 kJ/mol, respectively. The pharmacokinetics of (A, B, C, and D) molecules were obtained by using ADMET predictions. Based on the above findings, the current work recommends four compounds as potential TP enzyme inhibitors that activate colorectal and breast cancers.

**Keywords:** Cancer; isatin; molecular modeling; thymidine phosphorylase (TP).

**Resumen.** La inhibición de la actividad de la enzima TP ayuda a tratar y controlar las enfermedades. En esta investigación, se utilizaron métodos computacionales para investigar una serie de treinta oxadiazoles basados en isatina como posibles inhibidores de TP. Se utilizó 3D-QSAR para diseñar cuatro derivados de isatinas (A, B, C y D) con alta actividad anticancerígena. Se utilizó el acoplamiento molecular para investigar los tipos de interacción entre los derivados de isatina diseñados (A, B, C y D) y la enzima TP (PDB: 4EAD); los resultados muestran que todos los compuestos tienen varios tipos de interacciones excitantes sin interacciones desfavorables, pero solo los compuestos A y B tienen interacciones de enlace de hidrógeno convencionales como actividad de inhibición prometedora. La energía de enlace entre los compuestos (A, B, C y D) y la enzima TP se obtuvo mediante simulación dinámica molecular a 100 ns. Los compuestos A y B tenían una energía libre de enlace más sustancial que los compuestos C y D, con energías de enlace de -20,1374 +/- 0,1189 kJ/mol, -20,1897 +/- 0,1333 kJ/mol, -18,1344 +/- 0,1604 kJ/mol y 19,077 +/- 0,1549 kJ/mol, respectivamente. La farmacocinética de las moléculas (A, B, C y D) se obtuvo mediante predicciones ADMET. Con base en los hallazgos anteriores, recomendamos considerar cuatro compuestos como posibles inhibidores de la enzima TP que activan los cánceres colorrectales y de mama.

**Palabras clave:** Cáncer; isatina; docking molecular; timidina fosforilasa (TP).

## Introduction

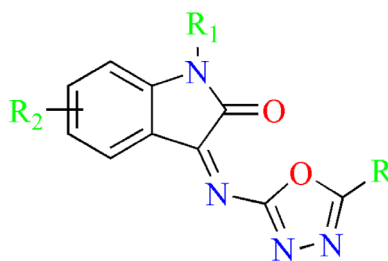
Cancer is a dangerous, deadly disease and is considered the second leading cause of premature death in the world after cardiovascular diseases [1–2]. The growth of cancer cells contributes to the spread of tumor cells to other organs by moving cancer cells through the blood vessels, a process called malignant disease [3–4]. The spread of cancer and its infecting various parts of the human body prompted researchers worldwide to find practical solutions to treat this disease, which exhausted the health sector and drained a lot of money [5]. TP is a nucleoside enzyme that plays an essential role in pyrimidine metabolism. It catalyzes thymidine conversion to thymine and 2-deoxy- $\alpha$ -D-ribose-1-phosphate (dRib-1-P) by a catabolic pathway. TP has been shown to promote tumor angiogenesis and is overexpressed in several human cancers, metastasis, invasion, immune response evasion, and resistance to apoptosis. Indeed, TP is used clinically against several cancer diseases, such as colon and metastatic breast cancer [6], because it is vital in activating capecitabine drugs against lung cancer and colorectal cancer [7–8]. Thymidine phosphorylase results in various pathological diseases such as rheumatoid arthritis, atherosclerosis, psoriasis, and inflammatory bowel disease [9]. Previous research investigations have revealed that isatin compounds have a wide range of biological activities, including anti-inflammatory [10], anti-HIV [11], antidepressant [12], anticonvulsant [13], antimalarial [14], antimicrobial [15], antiviral [16], antibacterial [17], and potential anticancer drugs [18–20]. In addition, isatin is widely distributed in the central nervous system and has been detected as a metabolite of epinephrine or tryptophan [21]. Isatin molecule was discovered by two chemists, Auguste Laurent and Otto Linné Erdmann [22]; it has a molecular formula of  $C_8H_5NO$ , a naturally occurring substance found in *Couroupita guianensis* plants of isatis [23–24].

In this work, computational studies based on 3D-QSAR, Comparative Molecular Similarity Indices Analysis, and Field Analysis (CoMSIA and CoMFA) [25–26] were used to understand the relationship between the structure of isatin-based oxadiazole and activity as TP inhibitors. Furthermore, four novel isatins were designed as effective inhibitors of TP inhibitors as potential anticancer drugs by utilizing the structural information obtained from the two models that exhibit excellent predictive potencies.

The pharmaceutical properties for designed (A, B, C, and D) molecules were explored by ADMET studies [27]. Furthermore, molecular dynamics simulations were performed for designs (A, B, C, and D) to investigate the stability of interactions with TP inhibitor enzyme.

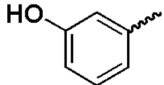
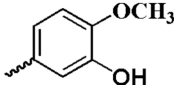
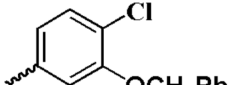
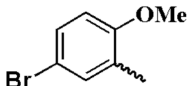
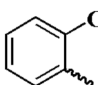
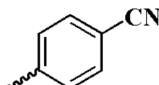
## Materials and methods

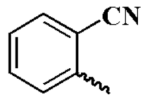
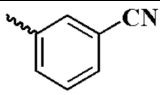
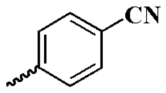
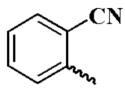
In the computational investigation of anticancer isatin-based oxadiazoles activity, the 30 compounds were divided into 2 groups: a training set of twenty-four molecules and six a test set of the remaining compounds. For the calculations, all experimental  $IC_{50}$  ( $\mu M$ ) activity values were transformed to the negative logarithm of  $pIC_{50}$ , the  $pIC_{50}$  calculated to use the formula ( $pIC_{50} = -\log IC_{50}$ ) and ( $1 \mu M = 1.0 \times 10^{-6} M$ ). Table 1 and Fig. 1 show the isatin-based oxadiazoles' structures and their  $pIC_{50}$  biological activity [9].



**Fig. 1.** Structures of isatin-based oxadiazole in the current study.

**Table 1.** Structures of isatin-based oxadiazole with TP inhibition activities.

N	R	R <sub>1</sub>	R <sub>2</sub>	pIC <sub>50</sub> (M)
1*		N-Isopropyl	H	5.11
2	-	N-Butyl	H	5.03
3	-	H	5-isopropyl	5.28
4	-	N-Pentyl	H	4.78
5	-	H	-	4.71
6		-	5-isopropyl	5.21
7	-	N-Isopropyl	H	5.33
8	-	N-Butyl	-	5.28
9*		H	5-isopropyl	4.84
10*	-	N-Isopropyl	H	4.95
11	-	N-Butyl	-	4.75
12		H	5-isopropyl	4.31
13	-	N-Isopropyl	H	4.54
14	-	N-Butyl	-	4.41
15	-	N-Pentyl	-	4.34
16	-	H	-	4.31
17		N-Isopropyl	-	4.60
18		N-Butyl	-	4.71
19*	-	N-Pentyl	-	4.46
20	-	H	5-isopropyl	4.57
21	-	N-Isopropyl	H	4.74

N	R	R <sub>1</sub>	R <sub>2</sub>	pIC <sub>50</sub> (M)
22		N-Butyl	-	4.43
23	-	N-Pentyl	-	4.58
24	-	H	5-isopropyl	4.66
25		H	-	4.47
26*	-	N-Pentyl	H	4.46
27	-	N-Butyl	-	4.52
28	-	H	-	4.73
29*		-	-	4.75
30		-	-	4.79

### Minimization and alignment

The essential characteristic in 3D-QSAR investigations is molecular alignment [28]. Sybyl was used to study molecular structures, then reduced using the Tripos Force Field [29] with 0.01 kcal/mol gradient convergence criteria and Gasteiger–Hückel charges, as well as the conjugate gradient approach. The Sybyl software was utilized to align the isatin compounds by using the most active molecule **C7** template.

### QSAR Studies

#### CoMFA and CoMSIA contours

To determine CoMFA and CoMSIA contour as QSAR keys, the electrostatic (E) and steric (S) fields are observed on the first contour. Whereas in the second contour, the hydrogen bond acceptor (A), hydrogen bond donor (D), and hydrophobic (H) fields are observed. The calculations are made at 2.0 Å for each lattice, and Gasteiger–Hückel method is loaded for each structure [30].

### PLS validations

Partial Least Squares (PLS) is an application used to predict a linear correlation between anticancer activity values and the two contours by obtaining the Leave-One-Out (LOO) approach was used to obtain the optimal number of components (N) and the coefficient of cross-validation correlation ( $Q^2$ ) [31]. The non-cross-validation approach yielded the correlation coefficient ( $R^2$ ), F-test value (F), and standard error of the estimate (SEE). At the same time, external validation was also used to evaluate the testing sets by ( $r^2_{\text{ext}} > 0.6$ ), the needed criterion.

### External validation

The criteria of Golbraikh, Tropsha, and Roy [32] are relationships to create reliable models and can be used to predict molecular activities for the test set. Table 4 below shows all the criteria results  $r^2_{\text{ext}} = 1 -$

PRESS  
SD

PRESS: Indicates squared deviations between predicted and measured values.

SD: The total of the squared deviations between the average activity of the test set and training set.

$$k' = \frac{\sum \left( \frac{Y_{\text{pred}} \times Y_{\text{test}}}{\sum (Y_{\text{test}})^2} \right)^2}{\sum (Y_{\text{pred}})^2}, k = \frac{\sum (Y_{\text{test}} \times Y_{\text{pred}})}{\sum (Y_{\text{pred}})^2}, r_0'^2 = 1 - \frac{\sum \left( \frac{Y_{\text{pred}} - k \times Y_{\text{pred}}}{\sum (Y_{\text{pred}} - k \times Y_{\text{pred}})} \right)^2}{\sum (Y_{\text{pred}} - k \times Y_{\text{pred}})^2}, r_0^2 = 1 - \frac{\sum (Y_{\text{pred/test}} - k \times Y_{\text{pred/test}})^2}{\sum (Y_{\text{pred/test}} - k \times Y_{\text{pred/test}})^2}$$

Y test and Y pred: Indicates the experimental and calculated values successively.

At zero intercepts, we start the calculation with K, K' then we can calculate  $r_0'^2$  and  $r_0^2$ . In addition to these external validation criteria, and in order to obtain a predictable and reliable model, the researchers have used another criterion called Roy [33], Roy's criteria are determined using the parameters,  $r_m^2$ ,  $\Delta r_0^2$ ,  $\Delta r_m^2$  and  $r_m'^2$ , both require the expressions below:

$$r_m^2 = r^2 \left( 1 - \sqrt{(r^2 - r_0^2)} \right); \quad r_m'^2 = r^2 \left( 1 - \sqrt{(r^2 - r_0'^2)} \right); \quad \Delta r_0^2 = r_0^2 - r_0'^2; \quad \Delta r_m^2 = r_m'^2 - r_m^2.$$

### Molecular docking

Molecular Docking was used to determine the interactions with ligands (A, B, C, and D) and the TP enzyme (4EAD) [34-35]. The preparation of Protein is the first step after downloading this Protein from a PDB (Protein Data Bank) database ([www.rcsb.org](http://www.rcsb.org)), then eliminating the water molecules of this receptor and adding polar hydrogens and Kohlman charges. In addition, the Surflex-dock technique available in Sybyl-x.2.0 was used for the docking protocol's protein and ligand preparation steps. Each complex of ((A, B, C, and D) and the TP enzyme (4EAD)) was investigated by the pymol program to be exported in a single file in pdb form [36]. The complex structures were studied by Discovery Studio in 2016 to know and see the types of interaction [37].

### ADMET properties

The term ADMET uses in silico techniques to better forecast and understand how medications affect the body. It can optimize clinical usage, reduce unwanted side effects, direct research toward development, and improve therapeutic options. The developed drugs' physicochemical characteristics were assessed using the SwissADME and pKCSM online programs [38]. The absorption, distribution, metabolism, excretion, and toxicities are examples of traditional pharmacokinetic parameters (ADMET) [39].

### Molecular dynamics simulation (MD)

The four complexes (A, B, C, and D) were chosen for MD simulation, and the Gromacs simulation package [40] was used, using a truncated octahedral box containing TIP3P Water molecules with Charmm36 force field [41-44]. To ensure a fully converged system, the NPT and NVT are fixed at 1000ps (1,000,000 steps) and 100ps (50,000 steps), using 0.1 and 0.2 fs, respectively. To eliminate any steric problems, the convergence was attained within the maximum force limit of 1000(KJ mol<sup>-1</sup> nm<sup>-1</sup>), the steepest descent method was used to do a depreciation for 5000 cycles, and the neutral solution was obtained with the addition of chlorine and potassium ions. The simulation was also carried out with a pressure (1 atm) and a temperature (300K) as a reference. They were controlled using Parrinello–Rahman barostat and Berendsen thermostat, respectively. In the following part and to obtain a time step (2 fs), the hydrogen atom lengths were held rigid at ideal bond lengths using the Linear Constraint Solver (lincs) algorithm. The systems were subjected to free 100 ns production simulations, with the Particle Mesh Ewald (PME) to calculate the electrostatic interactions, the verlet scheme for calculating non-bonded interactions, and Periodic Boundary Conditions (PBC) for all x, y, and z directions.

### Binding energy calculations

The energies of complexes play a critical part in many biological functions. Thus, it is crucial to figure out what they are. The binding energies of interactions were determined using the molecular mechanics

generalized Born surface area (MM-GBSA) technique and the total energy was obtained using the equation below:

$$\Delta G_{bind} = \Delta G_{RL} - \Delta G_R - \Delta G_L \quad \text{and} \quad \Delta G_{bind} = \Delta H - T\Delta S = \Delta E_{MM} + \Delta G_{Sol} - T\Delta S$$

## Experimental

### Materials and methods

#### The alignment of molecules

The alignment of molecules is the most precise method to explore molecules databases belonging to the same families is the alignment of the molecules, where the alignment cores are illustrated in Fig. 2.

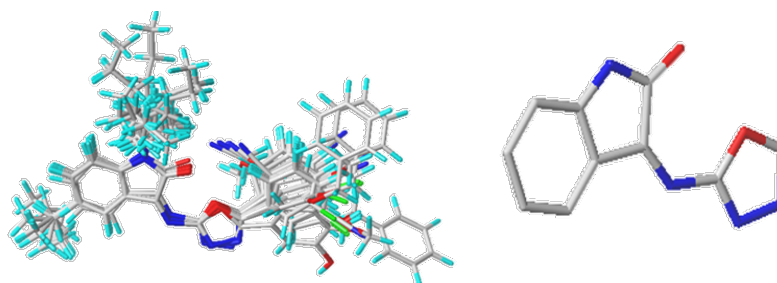


**Fig. 2.** Alignment compounds left, a core right.

### 3D-QSAR results

The compounds are separated into two groups: a training set of 24 and a test set of six compounds. The appropriate values for the COMFA model are  $R^2$  (0.93),  $F$  (91.51),  $Q^2$  (0.56), and  $S_{cv}$  (0.09). With three being the ideal number of indicators, the external validation gave the value of  $r^2_{ext}$  (0.98), the steric ( $S$ ) contribution was 65%, but the electrostatic ( $E$ ) did not exceed 35%.

CoMSIA's results suggest that non-cross-validated  $R^2$  (0.85),  $Q^2$  (0.60), a three-component optimum number,  $F$  (39.55),  $S_{cv}$  (0.13), as well as solid regard for external validation  $r^2_{ext}$  (0.98), all values are acceptable. The contributions of the steric ( $S$ ), hydrophobic ( $H$ ), electrostatic ( $E$ ), H-donor ( $D$ ), and acceptor ( $A$ ) fields were 24 %, 20 %, 13 %, 10 %, and 33 %, respectively, indicating that the H-bond acceptor, steric, and hydrophobic fields are essential in this contour. Table 2 shows the statistical findings of the models, whereas Table 3 and Fig. 3 shows the expected and actual values of  $pIC_{50}$ . The difference between these values is not higher (at most 1). It indicates that these calculations are reliable.

**Table 2.** The study results.

Contours	$R^2$	$Q^2$	$S_{cv}$	$F$	$N$	$r^2_{ext}$	$S$	$E$	$H$	$D$	$A$
CoMFA	0.93	0.56	0.09	91.51	3	0.98	0.65	0.35	-	-	-
CoMSIA	0.85	0.60	0.13	39.55	3	0.98	0.24	0.13	0.20	0.10	0.33

**Table 3.** The pIC<sub>50</sub> is the actual and predicted value.

N°	pIC <sub>50</sub> (M)	CoMFA		CoMSIA	
		Predicted	Residuals	Predicted	Residuals
1*	5.11	5.11	0.00	5.06	0.05
2	5.03	5.03	0.00	5.04	-0.01
3	5.28	5.13	0.14	5.30	-0.02
4	4.78	4.84	-0.06	4.83	-0.05
5	4.71	4.67	0.04	4.86	-0.29
6	5.21	5.23	-0.02	5.21	-0.01
7	5.33	5.36	-0.04	5.37	-0.04
8	5.28	5.32	-0.04	5.29	-0.01
9*	4.84	4.88	-0.04	4.88	-0.04
10*	4.95	4.96	-0.01	4.93	0.02
11	4.75	4.75	0.01	4.75	0.01
12	4.31	4.33	-0.02	4.34	-0.02
13	4.54	4.52	0.02	4.48	0.06
14	4.41	4.39	0.03	4.37	0.04
15	4.34	4.38	-0.05	4.36	-0.03
16	4.31	4.32	-0.01	4.31	0.00
17	4.60	4.62	-0.02	4.63	-0.03
18	4.71	4.70	0.00	4.71	-0.01
19*	4.46	4.42	0.04	4.44	0.02
20	4.57	4.68	-0.11	4.71	-0.14
21	4.74	4.76	-0.02	4.77	-0.03
22	4.43	4.43	0.00	4.45	-0.02
23	4.58	4.52	0.06	4.52	0.06
24	4.66	4.63	0.03	4.64	0.02
25	4.47	4.45	0.02	4.44	0.02
26*	4.46	4.54	-0.08	4.53	-0.07
27	4.52	4.64	-0.12	4.65	-0.13

N°	pIC <sub>50</sub> (M)	CoMFA		CoMSIA	
		Predicted	Residuals	Predicted	Residuals
28	4.73	4.63	0.10	4.75	-0.02
29*	4.75	4.67	0.07	4.68	0.06
30	4.79	4.77	0.02	4.79	0.00

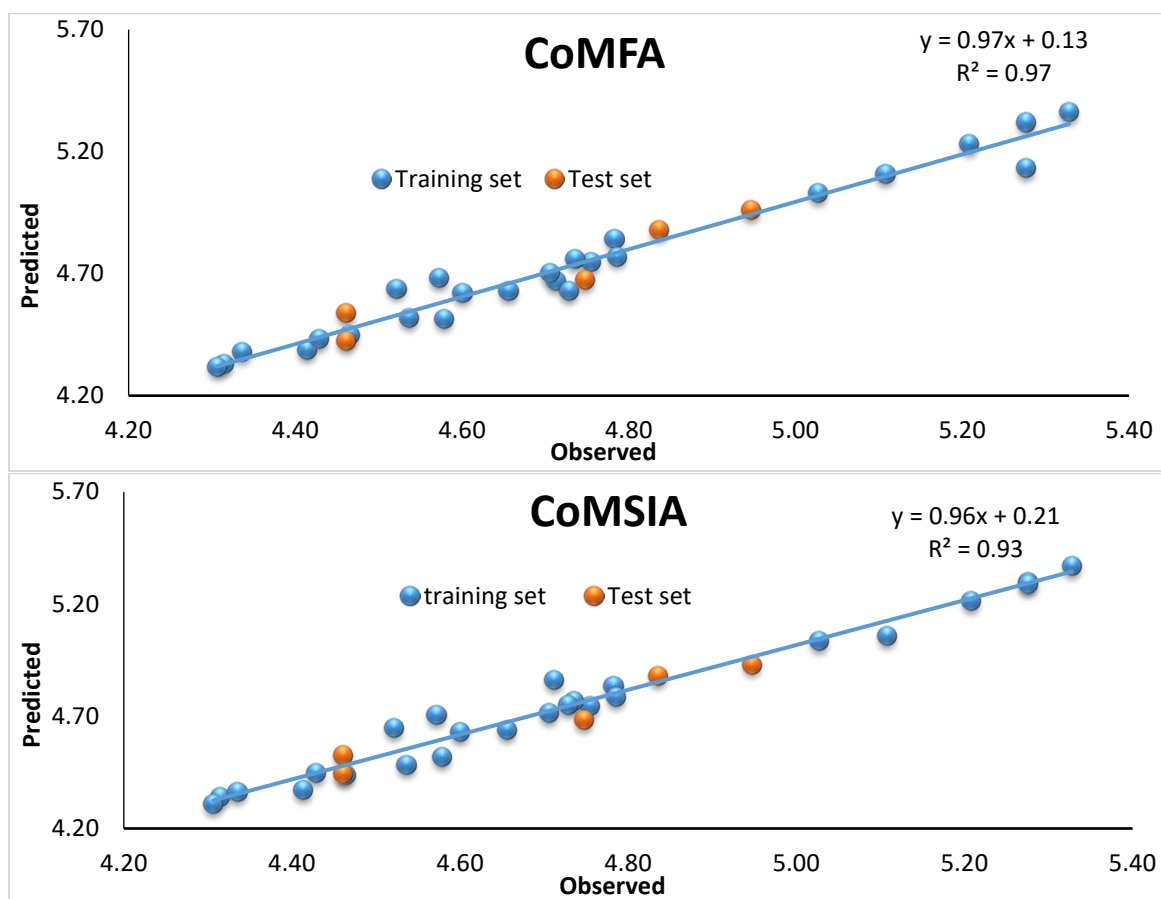


**Fig. 3** Observed and predicted pIC<sub>50</sub> of all compounds employed in constructing CoMSIA and CoMFA contours.

### Graphical interpretation

The contours were generated to determine the types of substituents that can decrease or increase activity. The Steric and electrostatic contours of COMFA are given in (Fig. 4(a) and (b)). In contrast, Hydrophobic, hydrogen bond donor and acceptor contours of COMSIA are displayed in (Fig. 5(a), (b), and (c)). In this study, all contours indicated the default 80 percent and 20 percent level contributions of the select and unfavored areas, respectively, utilizing the structure of compound 7 as a model.



### CoMFA contour

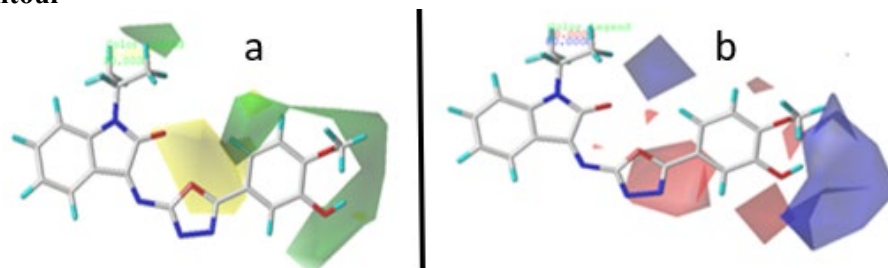


**Fig. 4** CoMFA analysis. **(a)** Steric, **(b)** Electrostatic.

In the steric field (Fig. 4(a)), the green color is seen near the phenyl ring of 1,3,4 oxadiazole parts and N-methyl. This indicates that the inhibitors with bulky molecules at these positions could increase the activity. So, compounds 2, 7, and 3 have higher activity than 5, 1, and 6.

In (Fig. 3(b)), the blue contour indicates that the electron donor groups near the 3-hydroxyl and methoxy groups of the phenyl part and N-alkylated methane group might have high activity, so compounds 3 and 8 are higher than 12 and 14.

### CoMSIA contour maps

CoMSIA contour explains H bond donor-acceptor (D-A) and hydrophobic (H), Fig. 5(a), (b), and (c) present the graphs of these fields, and the other fields (S, E) are the same in both contours.

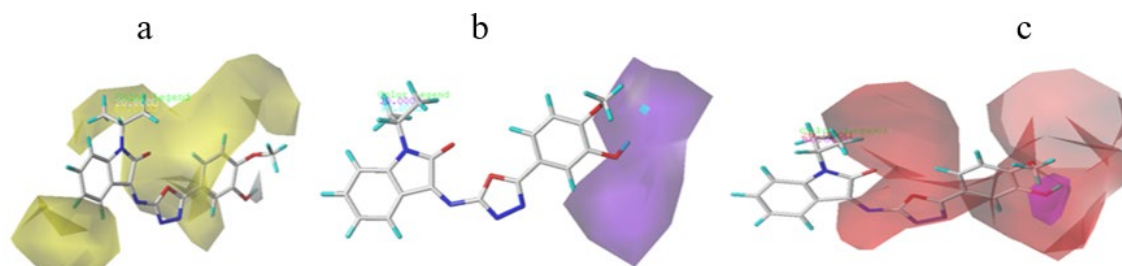


**Fig. 5.** CoMSIA analysis. **(a)** Hydrophobic, **(b)** H bond donor, **(c)** H bond acceptor fields.

The hydrophobic field was presented in (Fig. 5(a)) a large yellow color map that covers all the compounds except the 3-hydroxyl and methoxy on phenyl positions, which indicates that groups with hydrophobic character are favored more in these positions and might have enhanced activity. Compounds 2 and 4 are higher than 14 and 12. The purple color (Fig. 4(b)) appears near the OH, OCH<sub>3</sub>, and C2 substituents of the phenyl ring, revealing that the hydrogen bond donor is not preferred in this region, and the substituents of this type might decrease the activity. The Magenta contour (Fig. 4(c)) seen near the hydroxyl (OH) of the phenyl ring explains that substituents with hydrogen bond acceptor type can enhance the activity. In contrast, the red color around C1, C2, C3, C4, and C6 of the phenyl ring part and N-isopropyl reveals that hydrogen acceptor is not preferred in this region. This fraction is less than the others, so it will not be considered.

### External validation results

The Golbraikh, Roy, and Tropsha criteria are essential expressions for creating accurate models and applying them to the prediction of compound activities, as shown in Table 5, which lists the criteria results. In this table, the values of  $r_0'^2$  and  $r_0^2$  are more significant than 0.5; CoMFA has 0.962 and 0.965; CoMSIA has 0.971 and 0.999, respectively. That explains the ratio of the two values ( $\frac{r^2 - r_0'^2}{r^2}$ ,  $\frac{r^2 - r_0'^2}{r^2} < 0.1$ ) remains

less than 0.1, ( $r_m^2, r_m'^2 > 0.5$ ),  $\Delta r_0^2 < 0.3$  and  $\Delta r_m^2 < 0.2$  for both fields. In addition, the slopes  $k'$  and  $K$  have 1.012 and 1.013 in CoMFA. Moreover, CoMSIA has 0.991 and 0.995, respectively. The values are less than 1.15 and more significant than 0.85 in both contours. All parameters respect their margins of variation, which gives credibility to the present studied model to design new molecules, such as thymidine Phosphorylase (TP) inhibitors against cancer activity.

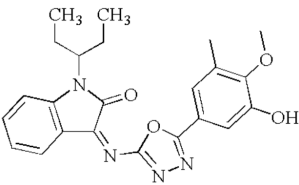
**Table 4.** The results of the Golbraikh Roy and Tropsha.

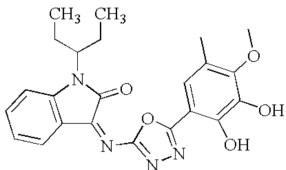
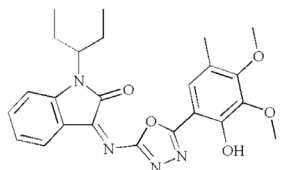
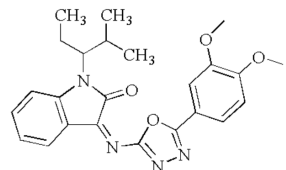
Criteria	Acceptance criteria		CoMFA	CoMSIA
Golbraikh and Tropsha	$r^2 \text{ ext}$	$r^2 > 0.6$	0.981	0.984
	$k$	$0.85 \leq k \leq 1.15$	1.013	0.995
	$r_0'^2$	$r_0'^2 > 0.5$	0.962	0.971
	$r_0^2$	$r_0^2 > 0.5$	0.965	0.999
	$k'$	$0.85 \leq k \leq 1.15$	1.012	0.991
	$\frac{r^2 - r_0^2}{r^2}$	$< 0.1$	0.016	-0.015
	$\frac{r^2 - r_0'^2}{r^2}$	$< 0.1$	0.019	0.013
Roy	$r_m'^2$	$r_m'^2 > 0.5$	0.845	0.871
	$r_m^2$	$r_m^2 > 0.5$	0.856	0.863
	$\Delta r_0^2$	$\Delta r_0^2 < 0.3$	0.003	0.028
	$\Delta r_m^2$	$\Delta r_m^2 < 0.2$	-0.011	0.008

### Newly designed compounds

The discovery of new drugs is one of the most complicated steps because this process involves several very complex steps. In this context, and according to the 3D QSAR study based on steric and H-bond acceptor fields, four more active compounds were designed with higher thymidine phosphorylase inhibitors against cancer activity. The pIC<sub>50</sub> values and structures of designed compounds are shown in Table 5.

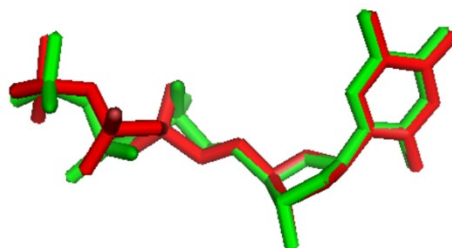
**Table 5.** Newly designed compounds.

N°	Compounds	The expected pIC <sub>50</sub> (M)	
		CoMFA	CoMSIA
A		5.545	5.540

N°	Compounds	The expected pIC <sub>50</sub> (M)	
		CoMFA	CoMSIA
<b>B</b>		5.422	5.420
<b>C</b>		5.346	5.341
<b>D</b>		5.323	5.319

### Docking results

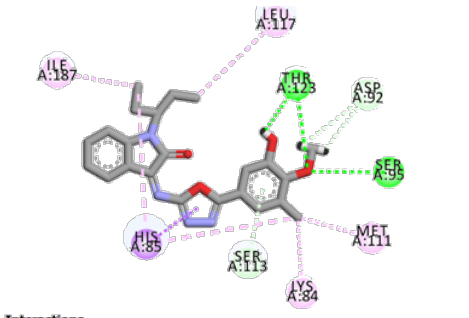
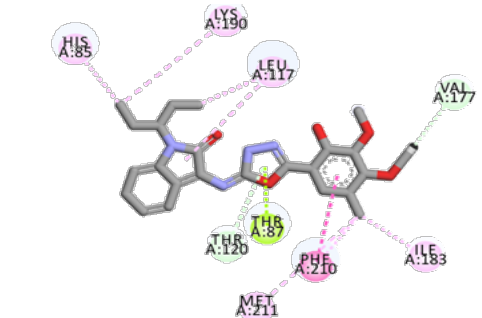
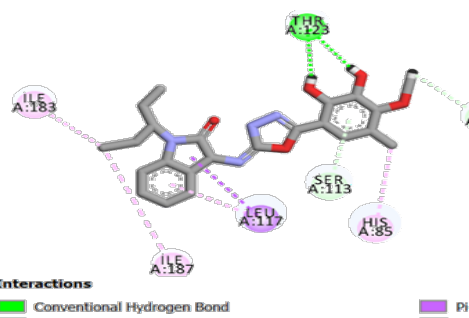
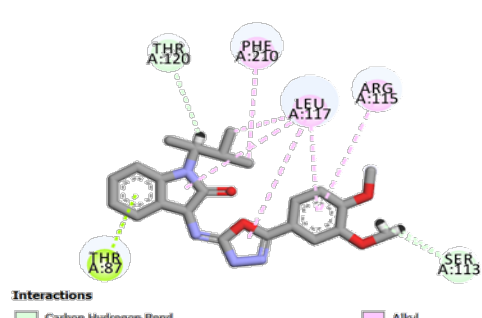
To verify its reliability, it is essential to study the redocking of co-crystal ligands before studying molecular docking. Fig. 6 shows the highly superimposable and consistent between the two conformations, and the RMSD was 0.861 Å. This indicates that the docking protocol that was performed was reliable and could be used for subsequent studies.



**Fig. 6.** Superimposition of the redocking pose (red) and the ligand pose in the co-crystal structure (green).

In an efficient state form (designed compounds-receptor), the Molecular Docking method was subjected to explore the interactions between the currently designed compounds and the TP inhibitor. The structure of thymidine phosphorylase (4EAD) was used as the receptor, and the compounds designed are the ligands; Table 6 summarizes the results of docking molecular.

**Table 6.** Results of docking molecules: show the interaction of designed compounds (A, B, C, and D) as ligands with the thymidine phosphorylase (receptor).

Nº	2D View	Nº	2D View
A	 <p><b>Interactions</b></p> <ul style="list-style-type: none"> <li>Conventional Hydrogen Bond</li> <li>Carbon Hydrogen Bond</li> <li>Pi-Donor Hydrogen Bond</li> <li>Pi-Sigma</li> <li>Pi-Pi T-shaped</li> <li>Alkyl</li> <li>Pi-Alkyl</li> </ul>	C	 <p><b>Interactions</b></p> <ul style="list-style-type: none"> <li>Carbon Hydrogen Bond</li> <li>Pi-Donor Hydrogen Bond</li> <li>Pi-Lone Pair</li> <li>Pi-Pi Stacked</li> <li>Alkyl</li> <li>Pi-Alkyl</li> </ul>
B	 <p><b>Interactions</b></p> <ul style="list-style-type: none"> <li>Conventional Hydrogen Bond</li> <li>Carbon Hydrogen Bond</li> <li>Pi-Donor Hydrogen Bond</li> <li>Pi-Sigma</li> <li>Alkyl</li> <li>Pi-Alkyl</li> </ul>	D	 <p><b>Interactions</b></p> <ul style="list-style-type: none"> <li>Carbon Hydrogen Bond</li> <li>Pi-Lone Pair</li> <li>Alkyl</li> <li>Pi-Alkyl</li> </ul>

The first component, A, demonstrates two conventional hydrogen bond interactions with THR123 and SER95, two mixed interactions between carbon H-bond and Pi-donor are ASP92 and SER113, one of pi-sigma with HIS85 residues, and four mixed interactions between Alkyl and Pi-Alkyl (LYS84, MET111, LEU117, ILE187). The second compound, B, has different types of interactions: one of conventional hydrogen bond interaction with THR123, two mixed interactions between carbon H-bond and Pi-donor (SER113, LYS84), one of pi-sigma is LEU117, and three mixed interactions between Alkyl and Pi-alkyl are HIS85, ILE187-183.

The third component, C, has diverse interactions: two mixed interactions between the carbon-hydrogen bond and pi-donor hydrogen bond (VAL177, THR120), one of pi-lone is THR87, and one of Pi-Pi stacked interactions is PHE 210. Five mixed interactions between Alkyl and pi-alkyl are HIS85, LYS190, LEU117, ILE183, and MET211. The fourth compound, D, has two interactions in the carbon-hydrogen bond (THR120 and SER113), one of pi-Lone is THR87, and three mixed interactions between Alkyl and pi-alkyl are PHE210, LEU117, and ARG115. The interaction types are summarized in Table 7. Compounds A and B have two groups (OH, OCH<sub>3</sub>) and (OH, OH) in the substituent R, respectively. These groups are close to each other; because of these groups, compound A has two interactions of type conventional hydrogen bond interactions with THR 123 and SER95. Moreover, compound B has a single bond of conventional hydrogen bond interaction with THR 123. The types of interaction increase the stability of compounds A and B compared to the rest of the compounds (C and D), but compound A is more stable compared to B. Compound C has bulky groups occupying most of the R substituent positions. At the same time, Compound D has only two OCH<sub>3</sub> groups, and one (CH<sub>3</sub>-CH-CH<sub>2</sub> (CH<sub>3</sub>)-CH<sub>3</sub>) group at the R1 substituent; these types of groups decrease the stability of compounds.

**Table 7.** The summary of the interaction types with the designed compounds and thymidine phosphorylase.

Interactions	Compounds			
	A	B	C	D
Conventional H-Bond	THR123, SER95	THR123		
Pi-Donor, H-bond/Carbon H-Bond	ASP92, SER113	SER113, LYS84	VAL177, THR120	HR120, SER113
Pi-Sigma, Pi-lone, Pi-Pi stacked	HIS85	LEU117	THR87, PHE210	THR87
Pi-Alkyl/ Alkyl	LYS84, MET111, LEU117, ILE187	HIS85, ILE187-183		

All the designed compounds do not have unfavorable interactions. The designed compound A has nine interactions, characterized by two essential interactions of the conventional hydrogen bond type. Moreover, compound B contains seven interactions in all, including one interaction of the conventional hydrogen bond. These interactions play an essential role in increasing the stability of their compounds. However, compounds C and D do not have any conventional hydrogen bond types. Therefore, it is crucial to determine the pharmaceutical properties of these compounds.

### ADMET prediction

ADMET method is used to understand the pharmacokinetics and determine the toxicity and safety of active molecules as potential drugs in the human body. Table 8 summarizes ADMET results of (A, B, C, and D) compounds.

**Table 8.** ADMET prediction results of (A, B, C, and D) compounds.

Model		Compounds			
		A	B	C	D
<b>Absorption (A)</b>					
<b>Intestinal absorption (human)</b>		100	90.61	94.84	96.97
<b>Distribution (D)</b>					
<b>Blood-brain barrier (logBB)</b>		-1.932	-0.752	-1.073	-1.994
<b>Volume of distribution Vdss(log L/kg)</b>		0.194	0.249	0.344	0.246
<b>Metabolism (M)</b>					
Substrate (CYP)	3A4	+	+	+	+
	2D6	-	-	-	-
Inhibition (CYP)	1A2	-	-	-	-
	2C19	+	-	-	+
	2C9	+	+	+	+
	2D6	-	-	-	-
	3A4	+	+	+	+

Model	Compounds			
	A	B	C	D
<b>Excretion (E)</b>				
<b>Clearance (log ml/min/kg)</b>	0.66	0.59	0.53	0.65
<b>AMES toxicity</b>	-	-	-	-

The absorption of active molecules by the human intestinal system is indicated by the letter A, computed by unit (% Absorbed). All molecules have a value closer to 100 %, indicating that this behavior is highly favorable to the human gastrointestinal intestine [45]. The second letter, D, indicates distribution; it is generally based on the (logBB) and VDss (log L/kg) that show the pathway of introducing drugs into the central nervous system is dangerous for the brain. Therefore, it is essential to eliminate the passage of drugs to the brain to protect the cerebral environment. The compounds A, D, and C have a value < -1, which indicates that they will not cross the blood-brain barrier.

Moreover, compound C has a  $-1 < -0.752 < 0.3$ , indicating an intermediate value. The second parameter studied in the distribution is the volume of distribution VDss (log L/kg); the higher the volume, the more the molecule will leave the vascular flow to diffuse in the body, but the brain has a protective barrier called the blood-brain barrier, the values of VDss vary between -0.15 and 0.45, if this value is lower than -0.15, it is considered a low. In contrast, if higher than 0.45, it is considered a high distribution. If  $-0.15 < \text{VDss} < 0.45$ , these are intermediate values. The third letter in the ADMET is M, which indicates metabolism; this shows the body's enzymatic system transforms the drug at the level of the liver; studies have shown that there are 57 CYP genes from 17 families in humans. Still, only CYPs (1A2, 2C9, 2C19, 2D6, and 3A4) are responsible for the biotransformation of 90 % of drugs. In our case, all compounds are not substrates or inhibitors of the cytochrome 2D6. Still, they are substrates and inhibitors of CYP3A4; for the rest, all compounds do not inhibit 1A2, but for cytochrome 2C19, only the B and C compounds are inhibitors. For the last cytochrome, all molecules are inhibitors of 2C9. The fourth letter, E, indicates excretion or clearance; it is a value that calculates the relationship between the rate of drug elimination and its concentration in the body. The results show a somewhat high value and are acceptable, and all predicted compounds are not toxic; this indicates that these compounds can be potent inhibitors of thymidine phosphorylase.

### MD simulation analysis

Calculations of RMSD, RMSF, Radius of Gyration Rg, Hydrogen Bonding, Average Center-of-Mass Distance, Contact Frequency (CF) Analysis, Potential energy, Pressure and Temperature, and MMGBSA Binding Energy were carried out to evaluate the study of each structure about time.

### Root mean square deviations (RMSD)

RMSD was used for the protein and ligand by using GROMACS program. RMSD graph (Fig. 7, Row 1), for the protein, the deviations of the proteins vary between 0.15 nm and 0.3 nm within 100ns of the simulation. These minimal deviations indicate that the proteins are stable throughout the simulation, which is the expected behavior of globular proteins. The RMSD of the ligand is shown in (Fig. 7, row 1); ligands A and B show fewer deviations in the last 80 ns of the simulations. These deviations are less compared to the deviations of ligands C and D. It indicates that ligands A and B showed higher stability than C and D. However, the minimum deviation for all ligands (less than 0.3 nm) for 100 ns indicates that the ligand can attack the active site of the protein.

### Root mean square fluctuations (RMSF)

RMSF was calculated for protein based on 'C-alpha' atoms using GROMACS program. (Fig. 7, Row 2) shows that the maximum fluctuation of all four complexes did not exceed 0.5 nm with residue 390 for complex C. Moreover, all four complexes showed similar dynamic fluctuations, indicating that these inhibitors have a similar binding mode with the enzyme Thymidine Phosphorylase.

### Radius of gyration (Rg)

The radius of gyration (Rg) was calculated for (A, B, C, and D) TP enzyme (4EAD)) complex based on 'C-alpha' atoms using GROMACS program, where the values were measured in nm. As (Fig. 7, Row 3) shows, ROG values for complex A stay between 2.26 nm and 2.34 nm or 22.6 Å and 23.4 Å. ROG for complex B increased values from the beginning of the simulation until 40ns, then stabilized after that, where its values stay between 22.9 Å and 23.2 Å with some slight fluctuations. After 10ns, ROG values after 10ns values 22.6 Å and 23.4 Å. ROG values complex D have an increasing pattern from the beginning of the simulation up to 40ns, stabilizing to values between 22.7 Å and 23.2 Å with some slight fluctuations. All four complexes show a very stable radius of gyration with a fluctuation of around 1-1.2 Å after 10ns, indicating the stability and compactness of the structure. The slight fluctuation around 1.0 Å Rog value during the MD simulation time indicates a slight opening and closing of the N and C terminal domains.

### Hydrogen bonds (HB)

The total number of HB formed between ligands (A, B, C, and D) and Protein (TP enzyme (4EAD)) during 100 ns of the simulation time is shown in (Fig. 9, Row 1), the maximum number of Hydrogen Bonds formed by TP and ligands A, B, C, and D are found to be 3, 4, 5, and 5 respectively.

### Average Center-of-Mass Distance

The average Center-of-Mass Distance between ligands (A, B, C, and D) and Protein (TP enzyme (4EAD)) during 100 ns of the simulation time is shown in (Fig. 9, Row 2). All compounds have unstable variations before 80 ns, but these graphs remain constant after this instant.

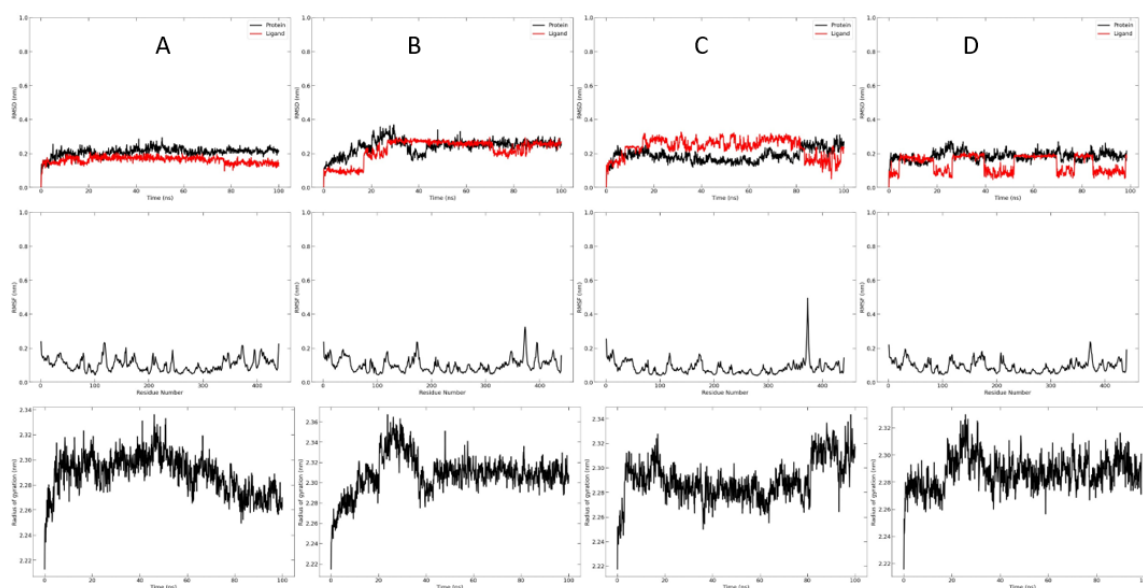


**Fig. 7.** From top to bottom: (1) RMSD, (2) RMSF, and (3) Rg of the complexes during 100ns MD simulation. Compounds A (Column A), B (Column B), C (Column C) and D (Column D).

After completing the proposed compounds' RMSD, RMSF, and Rg, Fig. 9 of the most ligands were added to compare (below). The average value of RMSD of both the ligand and protein studied was similar at all times of MD simulation analysis. We noticed they don't have any intersection (C7-protein), indicating that most compounds (C7) are unstable. Several fluctuations, e.g. characterize the mean RMSF values for the ligand (C7). The figure shows four fluctuations over 0.4 nm. In all systems, the RMSF for this compound is unstable.

Rg assessment. Rg analysis determines whether the protein under study is compact and folded during MD simulation. The overall results of Rg analysis show that the total Rg of compound 7 (C7) is comparatively

higher than the proposed compounds in each complex (Fig. 7). The Rg of C7 was initially lower but increased to 2.5 Å at 10 ns and then remained unstable up to 50 ns, after which the Rg of C7 reached a value between 2.6 Å and 2.65 Å, after 60 ns of simulation. We noticed that the Rg value in the C7 COMPOUND remained unstable throughout the MD simulation compared to the proposed compounds.

Generally, the RMSD, RMSF, and Rg results indicate that the four predicted complexes (A, B, C, and D) are stable and may serve as potential drug candidates as potential Thymidine Phosphorylase (TP) inhibitors against cancer activity.

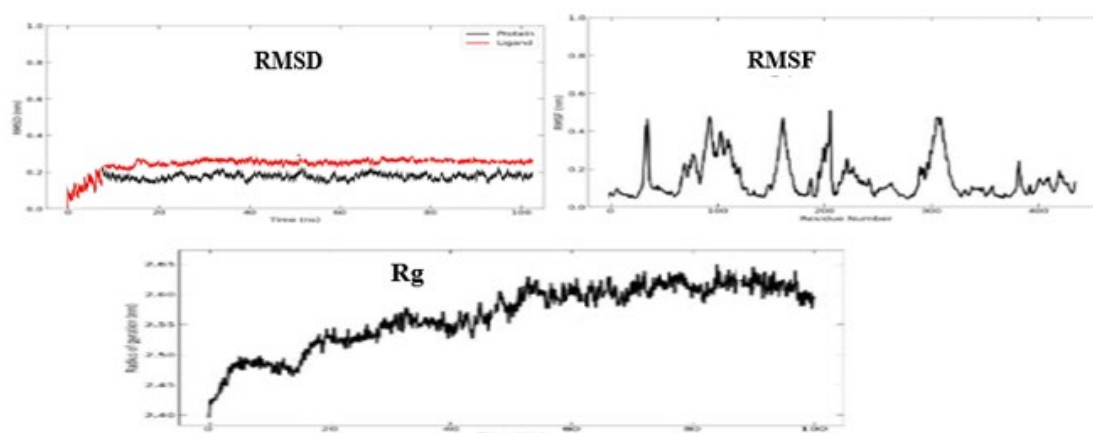


**Fig. 8.** RMSD, RMSF, and Rg of the complex (Compound7 (C7) - TP enzyme (4EAD)) during 100ns MD simulation.

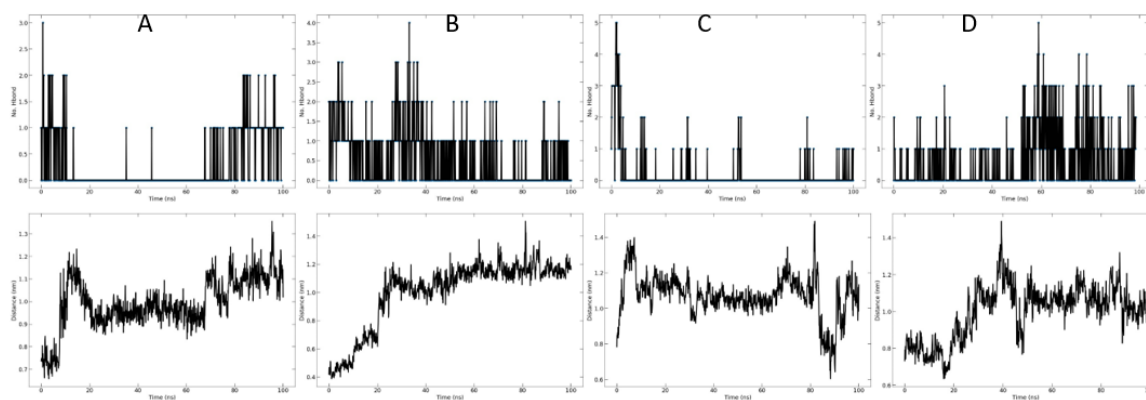


**Fig. 9.** From top to bottom: (1) Hydrogen Bonds (Protein-ligand) and (2) Average distance between Ligand and the Protein form of the complexes during 100ns MD simulation. Compounds A (Column A), B (Column B), C (Column C) and D (Column D).

### Percentage of Contact Frequency (CF)

The contact frequency (CF) analysis for (ligand (A, B, C, and D) and Protein (TP enzyme (4EAD))) complexes was done with 4 Å as a cutoff threshold. The names of residues in function to the CF percentage are presented in Fig. 10, where ligand D shows the highest contact frequency percentage.





The results showed that the A and the B complex had a solid binding free energy with the thymidine phosphorylase enzyme (TP), and their binding energies were  $-20.1374 \pm 0.1189$  kJ/mol and  $-20.1897 \pm 0.1333$  kJ/mol, respectively. In addition, the other compounds, C and D, had less binding energy with the thymidine phosphorylase enzyme (TP), and their binding energies were  $-18.1344 \pm 0.1604$  kJ/mol and  $-19.077 \pm 0.1549$  kJ/mol, respectively. The energy types are divided into *internal* energy, solvation energy, *electrostat* energy, and van der Waals energy. Among them, the solvation and electrostatic energy between the B and the TP enzyme was 15.0771 kJ/mol; this was the most critical factor in the binding energy. In addition, the energies of the compounds C, D, A, and TP enzymes have been classified as 14.2583, 13.5052, and 10.6882 kJ/mol, respectively. The final energy remains zero for all compounds. The van der Waals energy of compounds A, B, C, and D are -30.8256, -35.2668, -32.3926, and -32.5822 successively.

## Comparative study

The selective inhibition potential of Thymidine phosphorylase (TP) is the mainstay intervention in treating cancer activity in the absence of effective therapy for this severe disease. The design of new specific and selective inhibitors based on an isatin scaffold by applying computational methods to investigate the binding properties of isatin scaffold compounds as cancer inhibitors with target enzymes. In a previous study by *Jian-Bo et al.*, the quantitative structure-activity relationship of isatin-based oxadiazole derivatives as Thymidine Phosphorylase Inhibitors was investigated by 3D-QSAR and molecular docking study [46]. The present work investigated the cancer inhibitors' activity of Thymidine Phosphorylase by 3D-QSAR, molecular docking, and molecular dynamic simulation. Also, the pharmacokinetics and toxicity of designed compounds were visually screened by ADMETox study. In this work, we used a 3D-QSAR, Molecular Docking, ADME-Tox, and Molecular Dynamics Simulation analysis investigation of 30 compounds of anticancer isatin-based oxadiazoles activity, and each method has a vital role in this study.

## 3D QSAR

Used after the reliability check and the robustness for determining the nature of the substituents, which can decrease or increase the biological activities of the target compounds. Two contours determine the types of substituents, Comparative Molecular Similarity Indices Analysis and CoMSIA and Comparative Molecular Field Analysis CoMFA, which are essential to building QSAR.

## Molecular docking

It is an important method for exploring the interaction between ligands (A, B, C, and D) and the TP enzyme (4EAD).

## ADME-Tox

Drug research and development speed is accelerating, and the number of candidate compounds is increasing. It would waste a lot of resources to put them into experiments directly. Therefore, it is necessary to use computational modeling methods to evaluate their bioavailability and pharmacokinetics. The absorption, distribution, metabolism, excretion, and toxicities are examples of traditional pharmacokinetic parameters (ADMET) evaluation including Intestinal absorption (human), Blood-brain barrier (logBB), Volume of distribution V<sub>dss</sub>(log L/kg), cytochrome(CYP) enzyme inhibition and substrate, Clearance (log ml/min/kg), and AMES toxicity.

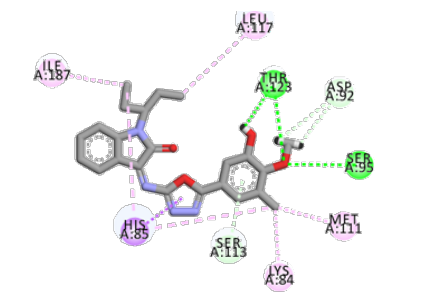
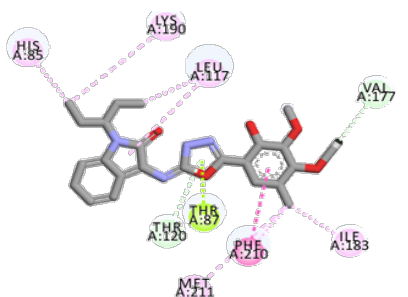
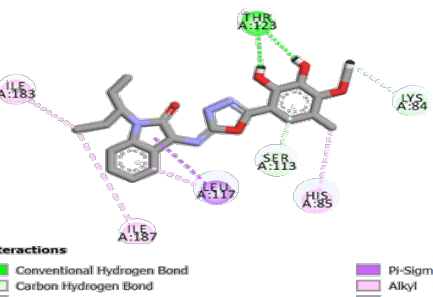
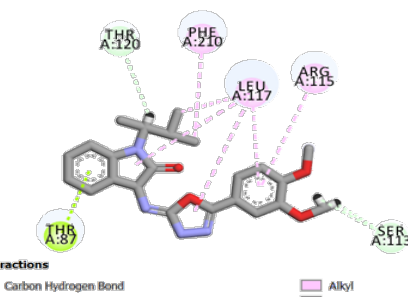
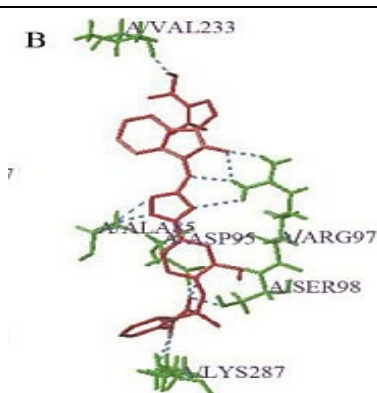
## Molecular dynamics (MD) simulation

MD simulation is essential for analyzing protein-ligand complexes. In this case, the ligands are the proposed compounds (A, B, C, and D), and the enzyme is Thymidine Phosphorylase TP (4EAD).

We found that just one work used 3D-QSAR, but in this work, they proposed other compounds that were different from our proposed compounds. The comparison between the results of both studies is summarized in Table 10. The docking result of the current study shows different types of interactions: conventional H-bond, Pi-Donor, H-bond/Carbon H-Bond, Pi-Sigma, Pi-lone, Pi-Pi stacked, and Pi-Alkyl/

Alkyl. In addition, the present work contains other complementary studies, ADMET prediction, and MD simulation analysis to study the properties and stability of the proposed compounds. The ADMET method is used to understand the pharmacokinetics and determine the toxicity and safety of active molecules as potential drugs in the human body. Section 3.6 (Table 8) summarizes the ADMET results (A, B, C, and D). The molecular dynamics simulation used binding stability between ligand- thymidine phosphorylase enzyme (TP) (compounds A, B, C, and D)- thymidine phosphorylase enzyme (TP) complexes. RMSD, RMSF, Radius of Gyration Rg, Hydrogen Bonding, Average Center-of-Mass Distance, Contact Frequency (CF) Analysis, and MMGBSA Binding Energy were carried out to assess the stability of each complex structure as shown in section 3.7 MD simulation analysis, figures 7, 8, 9, 10 and table 9.

**Table 10.** The comparison between the results of both studies.

Nº	Present work	Nº	Present work
A	 <p><b>Interactions</b></p> <ul style="list-style-type: none"> <li>Conventional Hydrogen Bond</li> <li>Carbon Hydrogen Bond</li> <li>Pi-Donor Hydrogen Bond</li> <li>Pi-Sigma</li> <li>Pi-Pi T-shaped</li> <li>Alkyl</li> <li>Pi-Alkyl</li> </ul>	C	 <p><b>Interactions</b></p> <ul style="list-style-type: none"> <li>Carbon Hydrogen Bond</li> <li>Pi-Donor Hydrogen Bond</li> <li>Pi-Lone Pair</li> <li>Pi-Pi Stacked</li> <li>Alkyl</li> <li>Pi-Alkyl</li> </ul>
B	 <p><b>Interactions</b></p> <ul style="list-style-type: none"> <li>Conventional Hydrogen Bond</li> <li>Carbon Hydrogen Bond</li> <li>Pi-Donor Hydrogen Bond</li> <li>Pi-Sigma</li> <li>Alkyl</li> <li>Pi-Alkyl</li> </ul>	D	 <p><b>Interactions</b></p> <ul style="list-style-type: none"> <li>Carbon Hydrogen Bond</li> <li>Pi-Lone Pair</li> <li>Alkyl</li> <li>Pi-Alkyl</li> </ul>
Other study			
(B) Hydrogen bond interaction between the newly designed molecule 1 and 5.			

In literature, we can find work using these computational chemistry methods on other derivatives and other activities. Generally, each molecule has a specific activity (anti-cancer, anti-diabetic, anti-inflammatory....). We used computational chemistry methods in several works, for example. In the work titled "3D-QSAR, molecular docking, ADMET, simulation dynamic, and retrosynthesis studies on new styrylquinolines derivatives against breast cancer [27]". We used other derivatives of styrylquinolines derivatives and their activity against breast cancer. In the second work titled "2-Oxoquinoline Arylaminothiazole Derivatives in Identifying Novel Potential Anticancer Agents by Applying 3D-QSAR, Docking, and Molecular Dynamics Simulation Studies [42]". We used other derivatives of 2-Oxoquinoline Arylaminothiazole. Generally, we have applied these methods to the design of new compounds against several diseases, and we have also applied them to the validation of compounds proposed.

## Conclusions

The 3D-QSAR study was used to determine the connection between molecules' structure and activity to determine the types of substituents that can increase the activity of the compounds. Both CoMFA and CoMSIA contours are the critical basis for designing new compounds. In this study, the two contours were used to design four molecules (A, B, C, and D), and the proposed compounds' binding mechanism and interaction with the active site of Thymidine Phosphorylase (TP) were studied using molecular Docking. Docking results showed that compound A is ranked first in terms of stability with two types of classical hydrogen bonding interactions, followed by compound B, which has only one kind of interaction. Two (A and B) compounds remain more stable than (C and D) because they do not have any classic hydrogen bond with TP inhibitor enzyme. The pharmacokinetic properties (ADMET) for (A, B, C, and D) compounds, including cell Blood-brain barrier, intestinal absorption, the volume of distribution, and metabolism, where the results were found to be non-Ames toxicity. Molecular dynamic (MD) results at 100 ns showed that all the compounds remained stable during the simulation. Current results encourage in vitro and in vivo studies of the designed isatin compounds as potent TP inhibitors.

## References

1. Ferlay, J.; Soerjomataram, I.; Dikshit, R.; Eser, S.; Mathers, C.; Rebelo, M.; Parkin, D. M.; Forman, D.; Bray, F. *Int. J. Cancer*. **2015**, 136, E359–E386. DOI: <https://doi.org/10.1002/ijc.29210>.
2. Nagai, H.; Kim, Y. H. *J. Thorac. Dis.* **2017**, 9, 448–451. DOI: <https://doi.org/10.21037/jtd.2017.02.75>.
3. Bronckaers, A.; Gago, F.; Balzarini, J.; Liekens, S. *Med. Res. Rev.* **2009**, 29, 903–953. DOI: <https://doi.org/10.1002/med.20159>.
4. Akiyama, S.; Furukawa, T.; Sumizawa, T.; Takebayashi, Y.; Nakajima, Y.; Shimaoka, S.; Haraguchi, M. *Cancer Sci.* **2004**, 95, 851–857. DOI: <https://doi.org/10.1111/j.1349-7006.2004.tb02193.x>.
5. Elamin, Y. Y.; Rafee, S.; Osman, N.; O'Byrne, K. J.; Gately, K. *Cancer Microenviron.* **2016**, 9, 33–43. DOI: <https://doi.org/10.1007/s12307-015-0173-y>.
6. Walko, C. M.; Lindley, C. *Ther.* **2005**, 27, 23–44. DOI: <https://doi.org/10.1016/j.clinthera.2005.01.005>.
7. Meropol, N. J.; Gold, P. J.; Diasio, R. B.; Andria, M.; Dhami, M.; Godfrey, T.; Kovatich, A. J.; Lund, K. A.; Mitchell, E.; Schwarting, R. *J. Clin. Oncol. Off. J. Am. Soc. Clin. Oncol.* **2006**, 24, 4069–4077. DOI: <https://doi.org/10.1200/JCO.2005.05.2084>.
8. Han, J.-Y.; Hong, E. K.; Lee, S. Y.; Yoon, S. M.; Lee, D. H.; Lee, J. S. *J. Clin. Pathol.* **2005**, 58, 650–654. DOI: <https://doi.org/10.1136/jcp.2004.022764>.
9. Javid, M. T.; Rahim, F.; Taha, M.; Nawaz, M.; Wadood, A.; Ali, M.; Mosaddik, A.; Shah, S. A. A.; Farooq, R. K. *Bioorganic Chem.* **2018**, 79, 323–333. DOI: <https://doi.org/10.1016/j.bioorg.2018.05.011>.

10. Sridhar, S. K.; Ramesh, A. *Biol. Pharm. Bull.* **2001**, *24*, 1149–1152. DOI: <https://doi.org/10.1248/bpb.24.1149>.
11. Selvam, P.; Muruges, N.; Chandramohan, M.; Debyser, Z.; Witvrouw, M. *Indian J. Pharm. Sci.* **2008**, *70*, 779–782. DOI: <https://doi.org/10.4103/0250-474X.49121>.
12. Rohini, R.; Reddy, P. M.; Shanker, K.; Kanthaiah, K.; Ravinder, V.; Hu, A. *Arch. Pharm. Res.* **2011**, *34*, 1077–1084. DOI: <https://doi.org/10.1007/s12272-011-0705-z>.
13. Verma, M.; Pandeya, S. N.; Singh, K. N.; Stables, J. P. *Acta Pharm. Zagreb Croat.* **2004**, *54*, 49–56.
14. Raj, R.; Gut, J.; Rosenthal, P. J.; Kumar, V. *Bioorg. Med. Chem. Lett.* **2014**, *24*, 756–759. DOI: <https://doi.org/10.1016/j.bmcl.2013.12.109>.
15. Bharathi Dileepan, A. G.; Daniel Prakash, T.; Ganesh Kumar, A.; Shameela Rajam, P.; Violet Dhayabaran, V.; Rajaram, R. *J. Photochem. Photobiol. B.* **2018**, *183*, 191–200. DOI: <https://doi.org/10.1016/j.jphotobiol.2018.04.029>.
16. Zhang, M.-Z.; Chen, Q.; Yang, G.-F. *Eur. J. Med. Chem.* **2015**, *89*, 421–441. DOI: <https://doi.org/10.1016/j.ejmech.2014.10.065>.
17. Guo, H. *Eur. J. Med. Chem.* **2019**, *164*, 678–688. DOI: <https://doi.org/10.1016/j.ejmech.2018.12.017>.
18. Ibrahim, H. S.; Abou-Seri, S. M.; Tanc, M.; Elaasser, M. M.; Abdel-Aziz, H. A.; Supuran, C. T. *Eur. J. Med. Chem.* **2015**, *103*, 583–593. DOI: <https://doi.org/10.1016/j.ejmech.2015.09.021>.
19. Eldehna, W. M.; Altoukhy, A.; Mahrous, H.; Abdel-Aziz, H. A. *Eur. J. Med. Chem.* **2015**, *90*, 684–694. DOI: <https://doi.org/10.1016/j.ejmech.2014.12.010>.
20. Sharma, P.; Senwar, K. R.; Jeengar, M. K.; Reddy, T. S.; Naidu, V. G. M.; Kamal, A.; Shankaraiah, N. *Eur. J. Med. Chem.* **2015**, *104*, 11–24. DOI: <https://doi.org/10.1016/j.ejmech.2015.09.025>.
21. Kerzare, D.; Khedekar, P. J. *Pharm. Biosci. Res.* **2016**, *6*, 144–156.
22. Erdmann, O. L. *J. Für Prakt. Chem.* **1840**, *19*, 321–362. DOI: <https://doi.org/10.1002/prac.18400190161>.
23. Silva, J. F. M. da; Garden, S. J.; Pinto, A. C. J. *Braz. Chem. Soc.* **2001**, *12*, 273–324. DOI: <https://doi.org/10.1590/S0103-50532001000300002>.
24. Bergman, J.; Lindström, J.-O.; Tilstam, U. *Tetrahedron* **1985**, *41*, 2879–2881. DOI: [https://doi.org/10.1016/S0040-4020\(01\)96609-8](https://doi.org/10.1016/S0040-4020(01)96609-8).
25. Klebe, G.; Abraham, U.; Mietzner, T. *J. Med. Chem.* **1994**, *37*, 4130–4146. DOI: <https://doi.org/10.1021/jm00050a010>.
26. Cramer, R. D.; Patterson, D. E.; Bunce, J. D. *J. Am. Chem. Soc.* **1988**, *110*, 5959–5967. DOI: <https://doi.org/10.1021/ja00226a005>.
27. EL-Mernissi, R.; Alaqarbeh, M.; Khaldan, A.; Kara, M.; Al Kamaly, O.; Alnakhli, A. M.; Lakhlifi, T.; Sbai, A.; Ajana, M. A.; Bouachrine, M. *Open Chemistry.* **2024**, *22*, 1–20. DOI: <https://doi.org/10.1515/chem-2024-0041>.
28. EL-Mernissi, R.; EL Khatabi, K.; Khaldan, A.; El Mchichi, L.; Ajana, M. A.; Lakhlifi, T.; Bouachrine, M. *Mater. Today Proc.* **2021**, *45*, 7608–7614. DOI: <https://doi.org/10.1016/j.matpr.2021.03.080>.
29. Clark, M.; Cramer, R. D.; Van Opdenbosch, N. *Comput. Chem.* **1989**, *10*, 982–1012. DOI: <https://doi.org/10.1002/jcc.540100804>.
30. Purcell, W. P.; Singer, J. A. *J. Chem. Eng. Data* **1967**, *12*, 235–246. DOI: <https://doi.org/10.1021/jc60033a020>.
31. El-Mernissi, R.; El Khatabi, K.; Khaldan, A.; ElMchichi, L.; Ajana, M. A.; Lakhlifi, T.; Bouachrine, M. *Egypt. J. Chemistry.* **2022**, *65*, 9–18. DOI: <https://doi.org/10.21608/ejchem.2022.76000.3715>.
32. Golbraikh, A.; Tropsha, A. *Mol. Graph. Model.* **2002**, *20*, 269–276. DOI: [https://doi.org/10.1016/S1093-3263\(01\)00123-1](https://doi.org/10.1016/S1093-3263(01)00123-1).
33. Roy, P. P.; Leonard, J. T.; Roy, K. *Chemom. Intell. Lab. Syst.* **2008**, *90*, 31–42. DOI: <https://doi.org/10.1016/j.chemolab.2007.07.004>.
34. Edache, E. I.; Uzairu, A.; Mamza, P. A.; Shallangwa, G. A. *J. Mex. Chem. Soc.* **2022**, *66*. DOI: <https://doi.org/10.29356/jmcs.v66i4.1726>.

35. Ibrahim, M. T.; Uzairu, A.; Umar, A. B.; Bello, A. S.; Isyaku, Y. *J. Mex. Chem. Soc.* **2019**, 64. DOI: <https://doi.org/10.29356/jmcs.v64i1.1025>.
36. DeLano, W. L. DeLano. PyMOL Mol. Graph. Syst. DeLano Sci. San Carlos CA USA 2002
37. Discovery Studio Predictive Science Application | Dassault Systèmes BIOVIA <https://www.3dsbiovia.com/products/collaborative-science/biovia-discovery-studio/>, accessed in February 2020.
38. Daina, A.; Michielin, O.; Zoete, V. *Sci. Rep.* **2017**, 7, 42717. DOI: <https://doi.org/10.1038/srep42717>.
39. El Khatabi, K.; Kumar, S.; El-Mernissi, R.; Singh, A. K.; Ajana, M. A.; Lakhlifi, T.; Bouachrine, M. *J. Biomol. Struct. Dyn.* **2022**, 0, 1–15. DOI: <https://doi.org/10.1080/07391102.2022.2134210>.
40. Van Der Spoel, D.; Lindahl, E.; Hess, B.; Groenhof, G.; Mark, A. E.; Berendsen, H. J. C. *J. Comput. Chem.* **2005**, 26, 1701–1718. DOI: <https://doi.org/10.1002/jcc.20291>.
41. Boonstra, S.; Onck, P. R.; Giessen, E. van der. *J. Phys. Chem. B* **2016**, 120, 3692–3698. <https://doi.org/10.1021/acs.jpcb.6b01316>.
42. El-Mernissi, R.; El Khatabi, K.; Khaldan, A.; Elmchichi, L.; Shahinozzaman, M.; Ajana, M.; Lakhlifi, T.; Bouachrine, M. *J. Mex. Chem. Soc.* **2021**, 66, 79–94. DOI: <https://doi.org/10.29356/jmcs.v66i1.1578>.
43. Lee, S.; Tran, A.; Allsopp, M.; Lim, J. B.; Hénin, J.; Klauda, J. B. *J. Phys. Chem. B* **2014**, 118, 547–556. <https://doi.org/10.1021/jp410344g>.
44. Hayes, J. M.; Skamnaki, V. T.; Archontis, G.; Lamprakis, C.; Sarrou, J.; Bischler, N.; Skaltsounis, A.-L.; Zographos, S. E.; Oikonomakos, N. G. *Funct. Bioinforma.* **2011**, 79, 703–719. DOI: <https://doi.org/10.1002/prot.22890>.
45. El-Mernissi, R.; El khatabi, K.; Khaldan, A.; Bouamrane, S.; ElMchichi, L.; Aziz Ajana, M.; Lakhlifi, T.; Bouachrine, M. *Orbital Electron. J. Chem.* **2022**, 14, 24–32. DOI: <https://doi.org/10.17807/orbital.v14i1.1659>.
46. Tong, J.-B.; Feng, Y.; Wang, T.-H.; Luo, D. *Chin. J. Anal. Chem.* **2021**, 49, e21046–e21054. [https://doi.org/10.1016/S1872-2040\(21\)60095-6](https://doi.org/10.1016/S1872-2040(21)60095-6).